Taurus Spitzer Legacy Project Data Release 2: Catalog and Mosaics for the Entire Survey

Deborah L. Padgett[1], Luisa M. Rebull[1], Caer-Eve McCabe[1], Alberto Noriega-Crespo[1] Sean Carey[1], & Tim Brooke[1]

1. Overview

The Taurus Spitzer Legacy project has mapped ≈44 square degrees of the Taurus star-formation region using the IRAC and MIPS cameras aboard the Spitzer Space Telescope. In this release, the team provides a bandmerged catalog of 269359 point sources with SNR > 15. Flux densities are reported for the 3.6, 4.5, 5.8, 8.0, 24 and 70 micron bands of IRAC and MIPS. Aperture photometry at three radii is provided for IRAC sources. PSF-fitting photometry is reported for MIPS flux densities. In addition, we provide Spitzer IRAC and MIPS mosaics for the entire Taurus survey, replacing the ones delivered in 2007. All mosaics are accompanied by coverage and uncertainty images.

Changes since last delivery:

- The remaining 30% of the data have been released. The released images and catalog now contain sources from the entire area surveyed in this Legacy program.
- The 24μm photometry has been re-normalized to a 13″radius aperture, resulting in the previously reported fluxes being revised upwards by 3%. In addition, the previous release quoted the formal *apex* uncertainties from the least-squares PRF fitting procedure. Further investigation has shown that the SNR provides a more secure uncertainty estimate, therefore, the 24μm uncertainties in the catalog have bene converted from the *apex* SNR. Due to these changes, the total number of sources at 24μm in the SNR > 15 catalog released with this document is smaller than in the previous release.
- The bandmerge process now includes a pre-merge of the 24 and 70 micron data sets prior to merging with the IRAC+2MASS catalog. Since any 70μm source is likely to also be detected at 24μm this process significantly reduces the chance that a 70μm source is spuriously associated with one of the shorter wavelength sources found at a much higher spatial density.

[1]Spitzer Science Center

2. Observations

2.1. IRAC

Approximately 44 square degrees of Taurus have been imaged with IRAC in 2005 and 2007. Because of the relative inefficiency of IRAC mapping for large areas and the absolute need to obtain at least two epochs of observations to eliminate asteroids, the Taurus Spitzer IRAC survey was limited to one 12 second high dynamic range frame per epoch. The region was mapped twice, providing a total of 25.2 seconds of integration time per point. The coverage of individual IRAC mosaics are illustrated in Figure 1 and Table 1.

2.2. MIPS

MIPS fast scans, with scan legs of 3 –6 degree length, were used to survey approximately 48 square degrees of Taurus during 2005 and 2007. Two epochs were obtained to identify the numerous asteroids, giving a total integration time of 30 seconds at 24 μm. Between the scan legs, the telescope was offset by 302 arcsec, resulting in a contiguous 24 μm map for each observing epoch, but unfilled maps at 70 μm and 160 μm. During the second epoch of observation, the map starting position was offset 150 arcsec in the cross scan direction from the previous scan map start position. It was also offset 16 arcsec along the scan direction. The cross-scan offset enabled us to fill in the missing half of the 70 μm array data during the second epoch, and the in-scan offset allowed filling (mostly) of the missing rows of 160 μm data which occur as a natural consequence of MIPS fast scan. For the Ge:Ga arrays, integration times are 15 sec for MIPS 70 μm and 3 sec for MIPS 160 μm. The coverage of individual MIPS mosaics are illustrated in Figure 2 and Table 2.

3. Data Reduction

3.1. IRAC

Post-processing was carried using Sean Carey's IRAC artifact mitigation software available in the SSC contributed software page[1]. The cleaning process starts with the basic calibrated data (BCDs) and deals mostly with bright sources artifacts. The steps in this post-processing are 1) hard saturations in the 12 second frames are identified and replaced

[1]http://ssc.spitzer.caltech.edu/archanaly/contributed/browse.html

with good data from the corresponding 0.6 second frame; 2) pixels bright enough to trigger artifacts are identifed and affected pixels are masked; 3) an estimate of the "true" sky for the masked pixels is made; 4) models of the artifacts are fitted to the difference between the data and sky estimate for the masked pixels; 5) the masked pixels are updated using the model fit.

Since the history-dependent temporal bias variations (first-frame effect) are quite apparent as a left to right slope in the 5.8 micron BCDs, a delta-dark (created through a robust median) of the image stack is applied. The median level of the 0.6 second frames are normalized to their 12 second counterparts. An estimate of the zodiacal light in each BCD is subtracted so that the two epochs for each field can be mosaicked together.

The previously released IRAC mosaics (v1.0) used only the dual outlier rejection method. Subsequent analysis of the mosaics found that a significant number of cosmic rays were passing through the outlier rejection and that occasionally, the fainter edges of stellar PSFs were being 'eaten.' After a number of tests, we have found that the combination of both box and dual outlier rejection will minimize both effects. All of the new mosaics (v2.0) are S14 pipeline data with box and dual outlier rejection employed.

The processed uncertainty maps are filtered, with each pixel replaced by the median of an 11 pixel wide box centered on the pixel. Special attention is paid to the edges of the uncertainty map – here the pixels are replaced with a boxcar smoothed version of the filtered uncertainty map. The processed BCDs, the filtered uncertainty maps, and the masks are then used to create a mosaic for each tile. For this purpose we use the SSC Post-BCD software package MOPEX (http://ssc.spitzer.caltech.edu/postbcd/mopex.html). The images are overlap corrected using *overlap.pl* and then mosaicked using *mosaic.pl*. Given that we only have 2 epochs of data, rejection of data outliers, such as radiation hits and moving objects, is important. We ran tests mosaicking the data using the dual outlier and box outlier methods. The dual outlier algorithm looks for >4 sigma outliers in each epoch. A comparison of the two epochs is done to see if the detected outlier is in fact a real source. Comparing the resulting mosaicks, we found that the dual outlier method failed to find a number of cosmic ray hits. In the box outlier method there were also clear instances when stellar PSFs were being 'eaten' by the outlier method. However, by using both the dual and box outlier rejection methods simultaneously we seem to have minimized the side-effects. Unfortunately, some cosmic ray hits on real astrophysical sources have persisted into the mosaics. We produced additional mosaics composed of the minimum value between the epochs to allow for identification and elimination of sources affected by radiation hits.

A single mosaic for each IRAC channel is not provided due to the large area of coverage involved; each individual mosaic tile has been released. The location for each mosaic is

shown in Figure 1 and the J2000 corner coordinates are listed in Table 1.

3.2. MIPS

MIPS images were processed by the Spitzer Science Center (SSC) using the standard pipeline to produce Basic Calibrated Data (BCD) images and related mask and uncertainty files. The SSC pipeline version was S14.4.0. For further information, see the MIPS Data Handbook, available at `http://ssc.spitzer.caltech.edu/mips/dh/`. The BCD images were corrected by us for some, but not all, instrumental signatures.

Our data reduction consisted of inspection of images for obvious artifacts, the creation of new masks for questionable pixels, and corrections for some of the known imaging defects. The masks were a merging of SSC pipeline pmask and dmask masks with bits deemed fatal into a simpler mask with 0 = good and 1 = bad. No new uncertainty files were created.

No attempt was made to explicitly remove cosmic rays or bright latent images from the BCD images. We used either the redundancy and outlier rejection in mosaicing, or inspection, to avoid mis-identifying these as point sources.

With the 24 μm array, a "jailbar" response pattern, repeating every fourth column sharing the same readout, is caused by bright sources and some cosmic ray hits. We applied an additive correction to each BCD data frame for any detectable fixed-amplitude jailbar pattern across the array, bringing lower columns up to the level of the highest columns. For some data, we corrected the jailbarring in sections: rows above and rows below a bright object.

"First frame" corrections were also applied. Scale factors were applied to frames at the start of a scan leg to bring them up to the median of subsequent frames.

Finally, 24 μm frames were median-combined with outlier rejection within an AOR to create "self-flats". These were needed to correct for residual low-level jailbarring, incompletely-corrected illumination patterns, a 1-2% gradient along the column direction, and occasional dark latent images. By "self-flatting", any true sky brightness gradient that is constant across the field covered by the median-combined images was also removed, i.e. scales of order 1 degree^2. To study emission on these scales, one must return to the original BCD data. In addition, spot patterns from dust on the pickoff mirror were present in the "0" frames of scan maps. These were divided out with separate spot-pattern flats created from the data.

No corrections were applied for improper "droop" corrections. This causes an overall

offset in frames containing saturating objects. Background matching routines were used to correct for offsets when creating the 24 μm mosaics. Other instrumental signatures, e.g., short-term dark latents, column and row pulldown effects, and streaks extending from bright objects, have not in general been corrected, though some preliminary additive corrections for column and row pulldown were done in a few cases.

Uncertainties resulting from these corrections to the pixel values are estimated to be typically $\lesssim$ 0.2 %, and the resulting uncertainties in point-source fluxes typically $\lesssim$ 0.03 mJy. This is usually small compared to other sources of uncertainties.

The Ge:Ga data from the 70 & 160μm arrays, is treated differently because of the time-dependent response of the arrays, the stims latencies and bright sources on stims artifacts. The steps to improve the Ge:Ga data are described 'MIPS Data Handbook V3.3.1' (http://ssc.spitzer.caltech.edu/mips/dh/index.html). Some additional steps have been applied to the 70μm data that have been used and tested in the processing of the MIPSGAL Legacy data (Paladini et al. 2009). These corrections are applied at the BCD level and before creating the final mosaic. The steps,in the order they are implemented are: (i) a 'delta flat' between stims, to correct time dependent gain variations, (ii) a stim outlier rejection, to remove corrupted stims during the calibration process, and (iii) an overlap correction to adjust minor surface brighthness offsets. However, this map is only useful for diffuse emission morphology, as point sources may be missing flux. The redistribution of flux by the smoothing process tends to reduce the flux density of compact/point source by as much $\sim$ 10%. Thus, the map is quite useful for the analysis of diffuse emission, but one should proceed cautiously with compact/point sources, using the original data to estimate their uncertainties.

The individual MIPS mosaics have been released. Figure 2 shows the MIPS mosaic locations overlayed on an IRAS 25μm image and the J2000 corner coordinates are listed in Table 2.

4. Photometry & Catalog Formation

4.1. IRAC

For the IRAC data, *apex* is run on the mosaics to generate source detection lists and IDL multi-aperture photometry done on each source detected by *apex*.

The *apex* settings were determined after running tests on two of the tiles (Tau 1 and Tau 2), varying the detection algorithm and the detection threshold. We found that the

best approach was to run the detection algorithm on the point source probability image created by APEX (use_psp_to_detect=1, input_type = image), with a detection threshold of 6. If the detection algorithm is run on the filtered image (psp=0), which is the point source probability image multiplied by the background subtracted image, an 'excess' of sources are found in channel 3 and 4, which are seen as a bump in the magnitude frequency distribution at the location of the peak. Applying the detection algorithm directly to the background subtracted image (psp=2), on the other hand, finds considerably fewer sources and the magnitude frequency distribution is more ragged than either other method.

Fluxes are measured in 3 different aperture sizes, 2 pixel, 5 pixel and 10 pixel radius circular apertures. The sky is measured in an annulus from 2–6, 5–10 and 10–20 pixels for the 2, 5 and 10 pixel aperture respectively. All fluxes are aperture corrected using the corrections listed in Table 5.7 of the IRAC data handbook. The source detection and photometry is applied to both the long and short integration mosaics. We use the 2 pixel aperture photometry throughout this document, the aperture corrections and zeropoints for which are listed in Table 2; if your focus is on particularly bright stars or extended objects, we recommend using the flux from a larger aperture. The outlier rejection process has done a reasonable job on removing cosmic rays, apart from the few instances when a cosmic ray hit is coincident with a stellar source. With only 2 epochs of data we do not have the redundancy to average these out in the mosaic process. Instead, we calculate the absolute minimum mosaic for each tile. Rather than combining the two separate epochs through an average of the measurements made at each unique location, the absolute minimum mosaic contains the minimum observed flux instead. To search for cases where a cosmic ray hit is coincident with a stellar source, we ran our aperture photometry code on the absolute minimum mosaic, and then source by source, compared the mean observed flux in a 2 pixel aperture (recorded in our catalog) with the absolute minimum observed flux. The majority of observed sources have fluxes that agree to within less than 0.1 mag, however, a small fraction appear to be quite discrepant. To identify these sources, the magnitude difference between the absolute minimum mosaic and the average mosaic is calculated. The sources are sorted by flux, and for each decade of flux, the median and standard deviation of the magnitude difference is calculated. Sources that have a magnitude difference greater than 4 sigma are flagged as suspicious. These sources (approximately 1%) remain in the catalog, but have a positive flag in the *iraccr* column. This analysis is run separately for each of the 4 IRAC channels.

The *apex detect* algorithm has a tendency to find multiple sources which can cause significant confusion at the bandmerging stage. Additionally, because our nominal fluxes are from the 2 pixel aperture photometry, any object which has a companion within 2 pixels will have a confused flux. The photometry lists are therefore cleaned of multiple sources prior

to the bandmerging. All SNR=1 sources are removed, and objects with a companion within 2 pixels has one of the sources removed. The source chosen for removal is the one with the lowest signal-to-noise ratio. Sources that have had a nearby companion removed from the catalog are flagged in the *iracdf* column of the catalog.

4.2. MIPS

Mosaicing and point-source extraction at 24 μm were done with the SSC's MOPEX package. Before mosaicing, the SSC's model estimate of the zodiacal light level, given in the data headers, was subtracted from each BCD frame. Then background correction was done. This determined the additive scale factors to apply to each frame to minimize the differences in the overlap regions. For Tau 1-4, the overlap corrector of the SSC's MOPEX package was used. For the other AORs, another program obtained from the MIPSGAL Legacy team provided slightly cleaner results. Single-epoch and combined mosaics were then created from the corrected 24 μm BCD data using MOPEX. Due to the large number of incompletely removed asteroids in the combined epoch 24 micron mosaics, we have delivered only the single epoch mosaics.

Estimates of the PRF (point response function) in each epoch were made from the mosaics with MOPEX, using 100–200 apparent point sources. The PRFs were used as input to MOPEX's point-source extraction. Other parameters used were similar to the defaults provided by the SSC. Point-source extraction was done on each epoch separately with a S/N cut of approximately 5. Bright latent star-like images were often mis-identified as point sources. These were removed by hand. Some obvious artifacts and dust clumps were also removed, though some of the remaining sources may in fact be dust clump peaks. For this 2nd data release, the 24μm PRF fluxes were normalized to match aperture-corrected aperture photometry in a 13″ radius aperture. Previous fluxes were revised upwards by 3% to match this calibration. Also, previously the adopted flux uncertainty was the *apex* delta flux, the formal uncertainty in the PRF-fit flux from the least squares fitting. Further investigation shows that the *apex* SNR outputed is the better measurement, so we take the SNR for each source and convert it back to a measurement uncertainty. These are the uncertainties now quoted in the catalog. These changes have resulted in a decrease in the number of 24μm sources identified in our catalog.

The final source extraction for the 70 μm catalog was performed on the post-processed final mosaic (see section 3.2). The extraction itself was carried out using APEX, and like in the IRAC extraction we used "psp_to_detect = 1" and "Input_Type = image_input", but with a detection threshold set to 4. The main issue with source extraction at 70 μm, even

after an intense artifact removal, is that small streak of "rowdy pixels" are confused by APEX as real sources. This problme takes place mostly on PRF-fitted SNR below 5, and that's why a SNR=6 was selected. A handful of faint unreliable sources were weeded out during the bandmerging process. At 70 μm some of the best known and bright objects are extended, and resolved by the 18″ 70 μm beam. Not surprisingly the PRF fitted photometry in these cases understimates the source flux density. For very bright sources, above 17Jy, non-linear effects can be an issue (see Gordon et al. 2007) as well. In two regimes the PRF-fitted photometry can not be blindly trusted, and caution is needed in interpreting results at this wavelength.

4.3. Bandmerging

All of the bandmerging was done strictly by position; no flux comparisons were used. The radial distance tolerance used for declaring a match was a function of wavelength. More details about the individual steps follow.

The first step in the bandmerging process was to assemble IRAC single-wavelength catalogs without duplicates. This process has in essence two parts. First, since the IRAC frames were 12s HDR, and separate extractions were done for the short and the long exposures, these source lists had to be merged to remove duplicates. We took all sources from the short frame brighter than a certain cutoff (magnitude 9.5, 9, 8, and 7 for channels 1, 2, 3, and 4, respectively) and with S/N > 5, and compared them (by position) to all of the sources from the long frame (also with S/N >5), letting the measured flux from the short frame take precedence over that from the long frame for these bright sources. All other fluxes were measured on the long frame. For the second part of this merging step, since the source extractions were done on a 'per AOR tile' basis, and some of the AOR tiles overlap, these individual tile extractions contained duplicates with objects found in adjacent tiles. Fluxes and flux errors for sources that had matches were calculated using a weighted average of the two measurements. For both merges, sources were considered a match if their positions agreed to within an arcsecond. In this fashion, we assembled a single catalog with unique sources at each of the IRAC wavelengths. The MIPS-24 source extractions were performed on global single epoch mosaics. The two epochs were then merged, leaving us with an asteroid-free MIPS-24 source list.

The next step in the bandmerging process was to merge across wavelengths. We started with the 2MASS catalog covering the region of interest. Then, we matched the IRAC-1 catalog to the 2MASS catalog with a tolerance of 1 arcsecond, preserving objects with IRAC-1 but no 2MASS fluxes. We then merged IRAC-2 to this 2MASS+IRAC-1 catalog,

again with a tolerance of 1 arcsecond. As a result of our low coverage, the incidence of false sources in IRAC frames is quite high. We had hoped that the bandmerging process would remove such sources, as the chances of a match across multiple wavelengths of a random event such as a cosmic ray is rather low. However, the surface density of false sources in specifically IRAC channels 1 and 2 is high enough that false hits later on in the bandmerging process is likely. As an additional screen for removing such false sources, we imposed an additional constraint at this point in the bandmerging process. Sources were only retained if they had a match between 2MASS, IRAC-1, and IRAC-2; e.g., sources with just IRAC-1 or just IRAC-2 were dropped. This necessarily removes sources in the "tabs" of 2-band IRAC coverage (bands 1 and 3 or 2 and 4) on the edges of the map, but it also removes hundreds of likely false sources from the catalog, which we regarded as an acceptable trade-off.

We continued with the bandmerging process, linking IRAC-3 to the master catalog, then IRAC-4, each with 1 arcsecond tolerance. For MIPS, the 70 μm source list was pre-merged to the 24 μm list with a radial tolerance of $10''$, before merging to the rest of the catalog. Because the spatial resolution of the 70 μm images is so much worse than the 2 μm images, often more than one NIR (or optical) source can be matched to the 70 μm source; however, it is extremely likely that if we detect a source at 70 μm, it will also appear at 24 μm, so by implementing the pre-merge of 24 and 70, we are preferentially matching the 70 μm sources to their true physical match. The MIPS 24-70 merged list was then merged to the IRAC+2MASS catalog with a radial tolerance of 2 arcseconds.

As the last step, we cleaned the catalog of likely false sources; single-band Spitzer detections were dropped as statistically unlikely, and MIPS-2 sources without MIPS-1 counterparts were dropped as likely noise. Finally, sources without Spitzer measurements (e.g., 2MASS only) were dropped.

The bandmerged catalog provided has a complete list of sources that exist in at least 2 Spitzer channels and have a signal to noise ratio of 15. Catalog statistics are shown in Table 4 and various color-magnitude and color-color relations for the catalog sources are shown in Figures 2 - 6.

5. References

Gordon, K., Engelbracht, C.W., Fadda, D., Stansberry, J., Wachter, S., et al. 2007, PASP, 119 1019

Paladini, R., Carey, S., Noriega-Crespo, A., Frayer, D., Ingalls, J., et al. 2009, in preparation.

Table 1. IRAC Tile Locations

Tile	AORs	Ra (J2000)	Dec (J2000)
tau1	11230208	72.70833,72.43333,71.265,71.574167	23.581389,26.470167,26.3715,23.48875
	11234048		
tau2	11230464	71.505833,71.200975,70.122333,70.458242	23.727028,26.617847,26.519144,23.636042
	11234304		
tau3-1	11230720	70.380167,70.154837,69.265708,69.505	23.569844,25.571072,25.489111,23.483817
	11234560		
tau3-2	11230976	70.15,69.915417,69.010833,69.266667	25.5585,27.559806,27.472331,25.472558
	11234816		
tau4-1	11231232	69.3,68.975,68.25,68.586667	25.327928,27.893806,27.817111,25.258306
	11235072		
tau4-2	11231488	69.59075,69.291958,68.584167,68.890667	22.883594,25.371389,25.294722,22.813836
	11235328		
tau5-1	11231744	68.494167,68.049583,67.318625,67.783333	25.746908,29.027503,28.950456,25.6722
	11235584		
tau5-2	11232000	68.8525,68.470833,67.760279,68.158333	22.892344,25.930019,25.853239,22.817364
	11235840		
tau6-1	11232256	67.796292,67.346483,66.709325,67.170417	25.752439,28.869836,28.798356,25.683006
	11236096		
tau6-2	11232512	68.186879,67.777871,67.157775,67.58125	22.817242,25.854236,25.782936,22.747614
	11236352		
tau7-1	11232768	67.140417,66.693333,66.056875,66.520792	25.722481,28.756769,28.679872,25.647617
	11236608		

Table 1—Continued

Tile	AORs	Ra (J2000)	Dec (J2000)
tau7-2	11233024	67.542446,67.130608,66.507842,66.93125	22.746522,25.789581,25.718272,22.679622
	11236864		
tau8-1	11233280	66.49675,66.035325,65.396242,65.871492	25.647114,28.6817,28.604772,25.572286
	11237120		
tau8-2	11233536	66.913021,66.487108,65.861742,66.299208	22.676108,25.714181,25.640139,22.606522
	11237376		
tau9	11233792	65.528521,65.333625,64.149558,64.358942	27.177489,28.533781,28.402867,27.042869
	11237632		
tau10	12914944	68.901292,68.688133,67.668454,67.894875	27.972647,29.979433,29.897331,27.892189
	12915712		
tau2scanA	19027712	65.391250,65.142917,64.174583,64.432083	28.541783,29.854792,29.715694,28.399086
tau2scanA	19027968		
tau2scanB1	19028224	66.058333,65.640000,64.784583,65.128750	24.640833,26.572639,26.433361,24.503250
tau2scanB1	19028480		
tau2scanB2	19028736	66.387917,66.064583,65.135000,65.471667	22.661556,24.608806,24.477775,22.527056
tau2scanB2	19028992		
tau2scanC1	19030272	64.779583,64.188750,63.494167,64.101250	26.536133,29.603111,29.495833,26.442772
tau2scanC1	19033856		
tau2scanC2	19030528	65.311667,64.761667,64.089167,64.652083	23.574806,26.613750,26.514944,23.475583
tau2scanC2	19034112		
tau2scanD	19032576	69.982083,69.773333,67.813333,68.037500	21.578194,23.148889,22.910972,21.348250
tau2scanD	19036160		

Table 1—Continued

Tile	AORs	Ra (J2000)	Dec (J2000)
tau2scanG1	19030784	64.084583,63.477083,62.784583,63.405417	26.702764,29.767000,29.659778,26.598611
tau2scanG1	19034368		
tau2scanG2	19031040	64.639583,64.067975,63.394583,63.985000	23.745500,26.784789,26.677806,23.649167
tau2scanG2	19034624		
taugap1-2	24243712	71.586750,71.228750,71.132625,71.4925	23.892194,26.577194,26.566889,23.881797
taugap2-3	24244224	70.452917,70.253458,70.290833,70.077500,	23.836242,25.280125,25.286889,26.729889,
taugap2-3	24243968	69.981250,70.196250,70.157917,70.359583	26.718914,25.275472,25.269361,23.825500
taugap4-5	24244736	68.899958,68.529583,68.603333,68.174583,	23.237139,25.666694,25.676833,28.191361,
taugap4-5	24244992	68.077833,68.494000,68.420000,68.806667	28.178894,25.753972,25.744444,23.225464
taugap4-10	24244480	68.979083,68.917875,68.143917,68.207083	27.869053,28.258517,28.151389,27.763611
taugap4-10	24246784		
taugap 6-7	24245504	67.611667,67.142083,67.236250,66.676250,	22.974722,25.836667,25.851556,28.836667,
taugap 6-7	24245248	66.578750,67.117500,67.025000,67.519167	28.822667,25.967972,25.955389,22.962250
taugap7-8	24245760	66.970833,66.470833,66.575000,65.994583,	22.928250,25.875556,25.891889,28.873333,
taugap7-8	24246016	65.895833,66.470833,66.366667,66.878333	28.859444,25.920278,25.906111,22.914972
taugap8-9	24246528	65.612500,65.462500,65.512500,65.350000,	27.292778,28.031111,28.040000,28.797500,
taugap8-9	24246272	65.255000,65.412500,65.362500,65.520417	28.781667,28.043889,28.035556,27.277222
tau2iracBgap	24243200	65.783333,65.600000,64.562500,64.758333	26.555833,27.473611,27.308056,26.390833
tau2iracBgap	24243456		
tau2iracB1-2	24242688	66.037500,66.020833,65.100,65.112500,	24.582500,24.667778,24.530278,24.444722,
tau2iracB1-2	24242944	65.999583,65.983333,65.058333,65.075000	24.817417,24.901944,24.758889,24.673611

Table 2. MIPS Scan Location

Scan name	AORs	Ra (J2000)				Dec (J2000)			
mosaic1	11225600	72.793667	72.409167	71.145833	71.562500	23.365417	26.774389	26.664722	23.240000
	11225856								
mosaic2	11226112	71.633333	71.220833	69.954167	70.404167	23.501389	26.928889	26.791667	23.371667
	11226368								
mosaic3	11226624	70.462500	69.870833	68.883333	69.512500	23.387778	27.801667	27.682500	23.274167
	11226880								
mosaic4	11227136	69.641667	68.895833	68.100000	68.879167	22.679444	28.085000	27.986111	22.582222
	11227392								
mosaic5	11227648	68.900000	67.958333	67.245833	68.216667	22.702778	29.113333	29.019444	22.615833
	11227904								
mosaic6	11228160	68.266667	67.295833	66.583333	67.591667	22.627222	29.031667	28.936389	22.537778
	11228416								
mosaic7	11228672	67.633333	66.637500	65.925000	66.954167	22.551111	28.951667	28.856111	22.459167
	11228928								
mosaic8	11229184	67.000000	65.983333	65.270833	66.320833	22.474444	28.871944	28.772778	22.376667
	11229440								
mosaic9	11229696	65.708333	65.400000	64.208333	64.541667	26.948333	28.835556	28.691667	26.797500
	11229952								
mosaic10	12915200	68.937500	68.683333	67.570833	67.908333	28.053889	30.064167	29.947500	27.945000
	12915456								
mosaicA	19026944	64.160417	64.393750	65.394167	65.168333	30.026111	28.129167	28.214639	30.114083
	19027456								

Table 2—Continued

Scan name	AORs	Ra (J2000)				Dec (J2000)			
mosaicB	19026688	64.695000	65.427083	67.354167	65.677500	26.991111	22.488472	22.613056	27.109444
	19027200								
mosaicC	19032832	63.584167	64.545833	65.225000	64.300000	29.695556	23.276944	23.363500	29.785278
	19032832								
mosaicD	19032320	67.733333	68.050000	70.057917	69.766667	23.046111	21.155694	21.428611	23.329167
	19035904								
mosaicG	19029504	62.857083	63.882500	64.561667	63.570833	29.856111	23.443056	23.533611	29.948611
	19033088								
mosaicABgap	24247040	65.937500	65.508333	64.333333	64.783333	26.424444	28.301389	28.086667	26.212778
	24247296								
mosaicBCgap	24247552	65.412500	64.808333	64.625000	65.233333	23.276667	26.620278	26.591111	23.245833
	24247808								
mosaics45gap	24248576	68.933333	68.170417	68.027083	68.794583	22.997750	27.333000	27.311917	22.979111
mosaic410gap	24248064	69.070833	68.800000	67.977083	68.275000	27.098889	29.000000	28.904167	27.001944
	24248320								

Table 3. Aperture Corrections & Zeropoints

channel	Aperture Correction	zeropoint
3.6	1.213	280.9
4.5	1.234	179.7
5.8	1.379	115.
8.0	1.584	64.13

Table 4. Catalog Composition

Channel (microns)	Number of sources	Minimum Flux Density μJy
total	269359	
3.6	267569	38
4.5	266711	38
5.8	53825	225
8.0	40153	217
24.	2546	2375
70.	693	40680

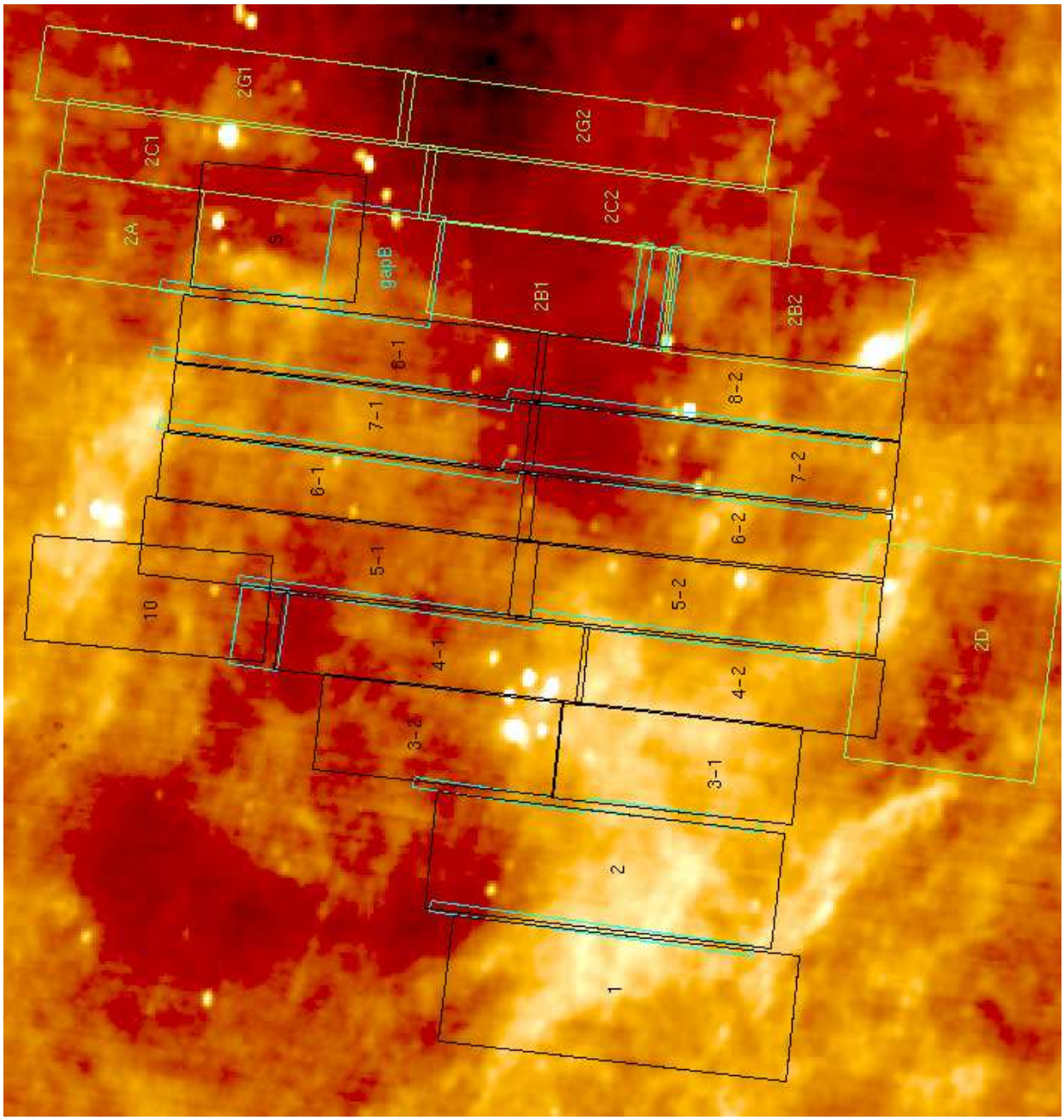

Fig. 1.— Location of the Taurus survey IRAC mosaics, overlayed on the IRAS 25 μm image. The polygons are color coded black for mosaics imaged during the TaurusI campaign, observed in 2005, green for mosaics observed during the TaurusII campaign in early 2007, and cyan for areas covered during our 'gap-filling' campaign in late 2007.

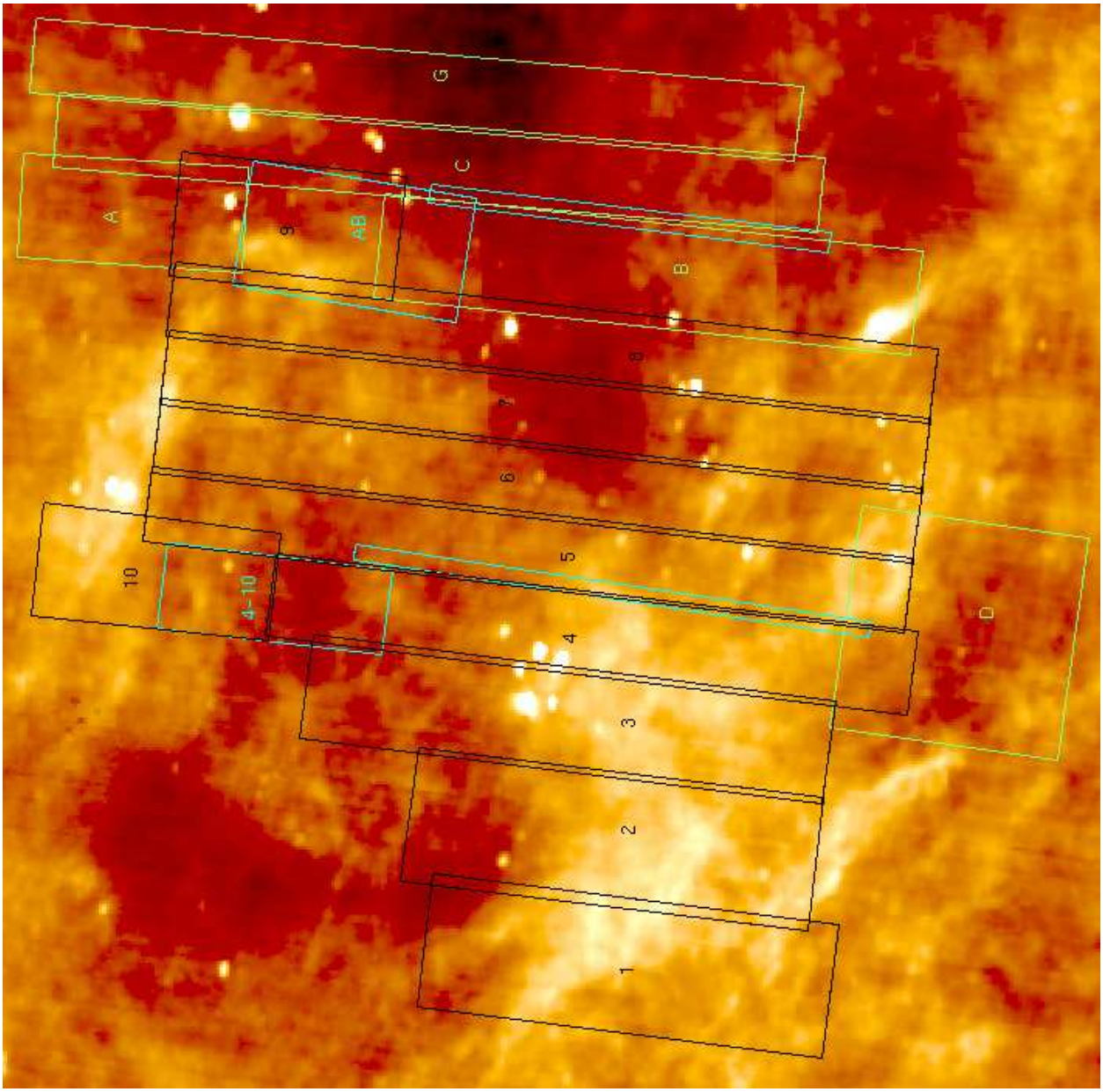

Fig. 2.— Similar to Figure 1, but for MIPS mosaics

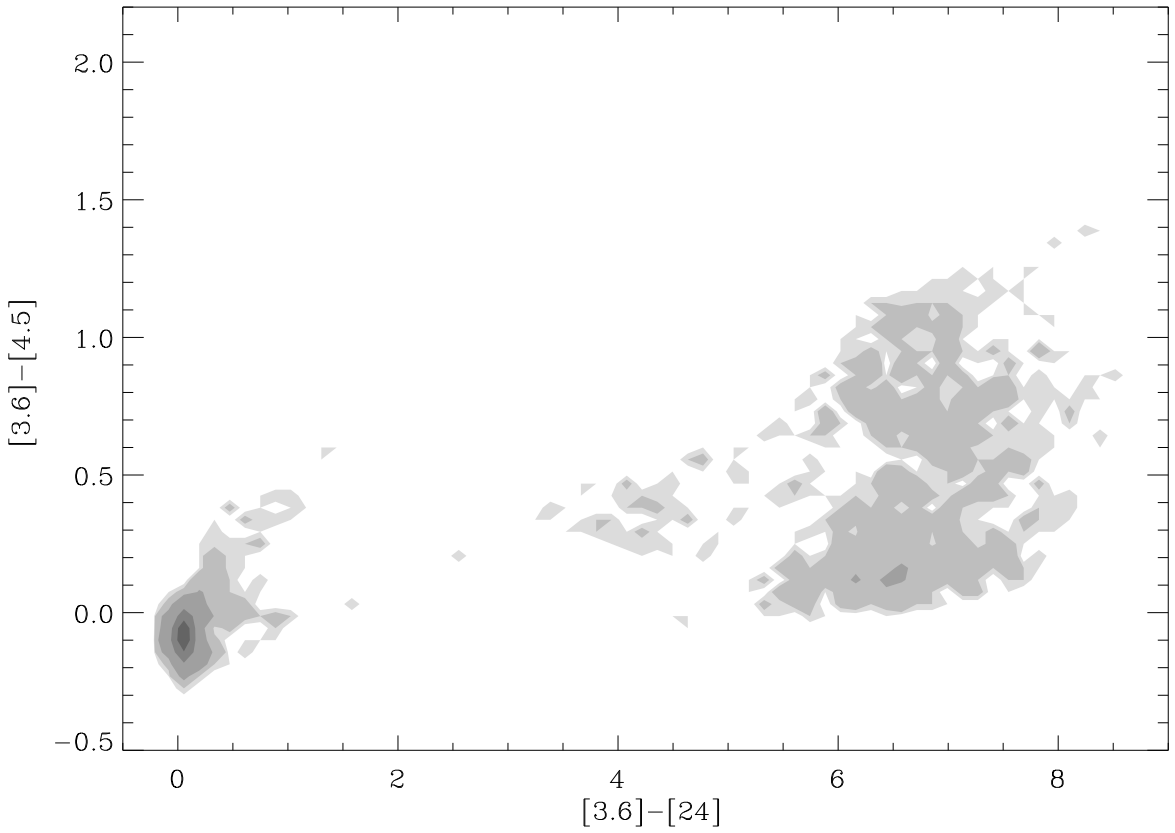

Fig. 3.— IRAC/MIPS Color-Color Plot for the 2nd delivery catalog: [3.6]-[4.5] vs. [3.6]-[24]. Greyscale contours indicate source density. Contour levels are 1, 2, 10, 50, 100 sources.

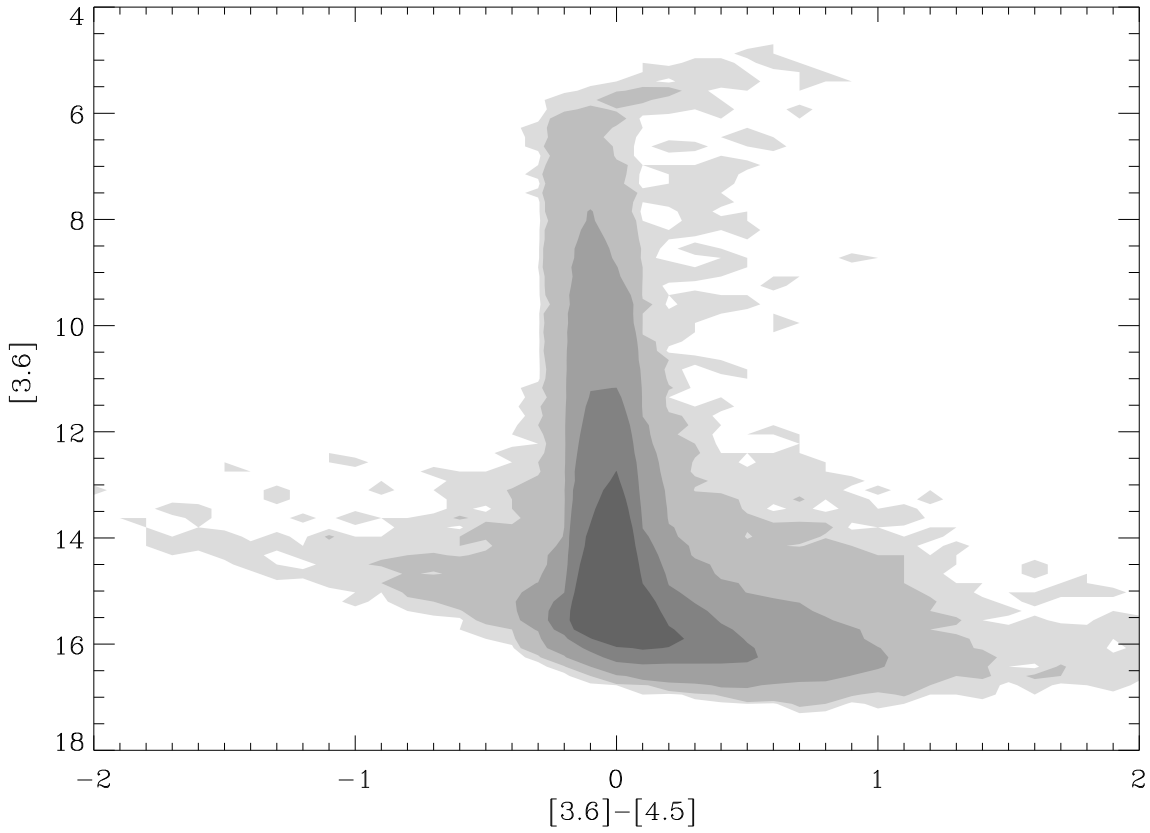

Fig. 4.— IRAC CMD for 2nd delivery catalog: [3.6] vs [3.6]-[4.5]. Contour levels are 1, 5, 50, 500, 2000 sources.

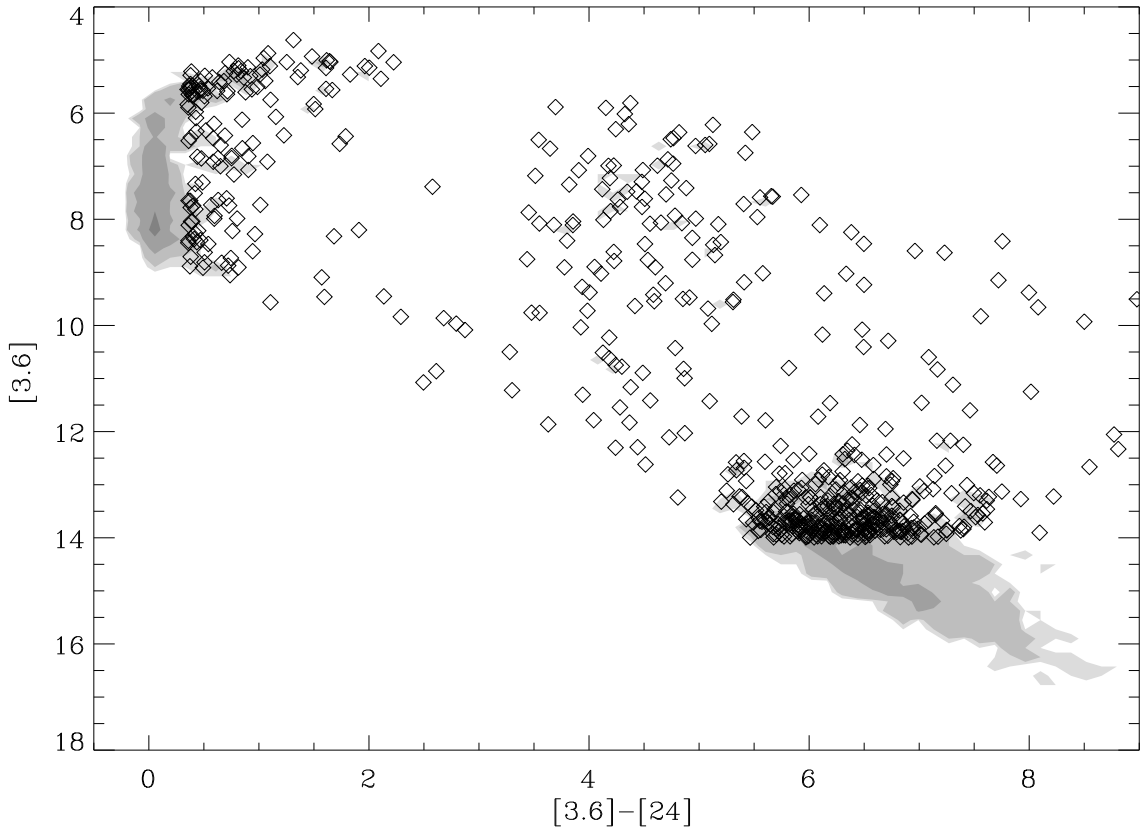

Fig. 5.— IRAC/MIPS CMD for 2nd delivery catalog: [3.6] vs [3.6]-[24]. Note that sources in the typical young stellar object regime are shown as points rather than contours. Contour levels are 1, 2, 10, 50, 100 sources.

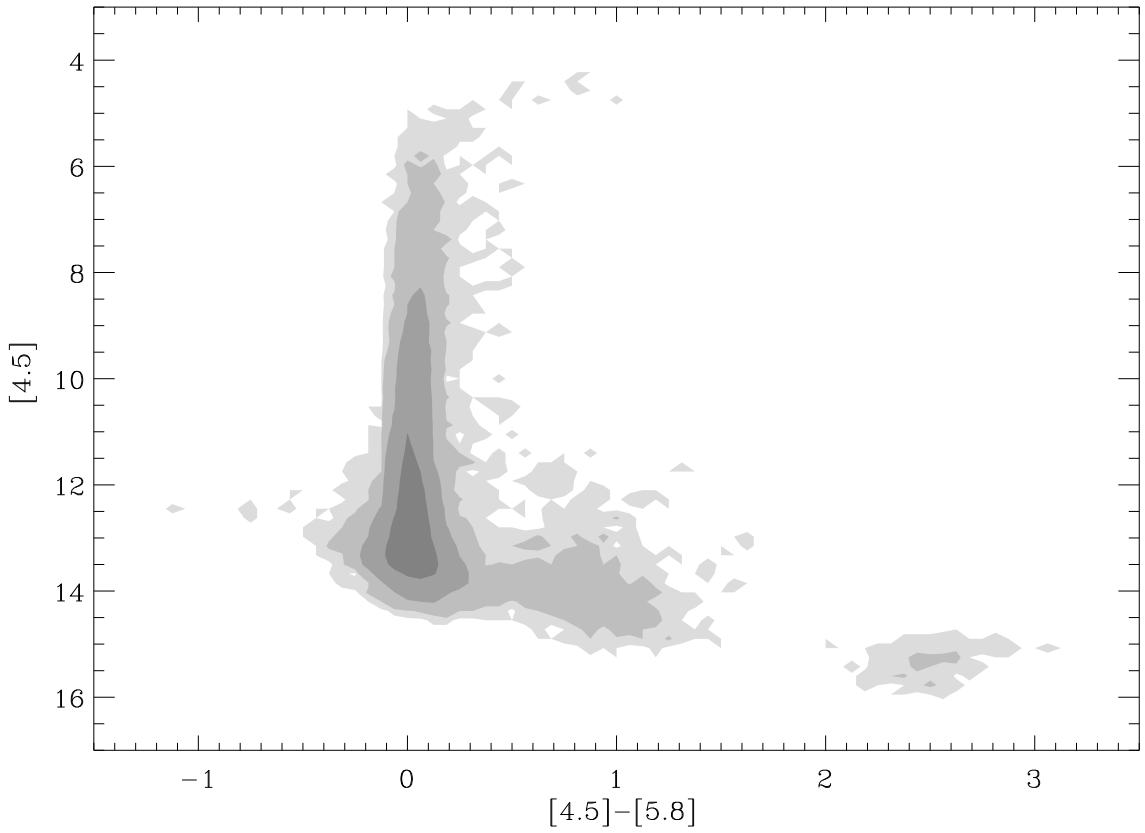

Fig. 6.— IRAC CMD for 2nd delivery catalog: [4.5] vs. [4.5]-[5.8]. Contours are 1, 5, 50, 500, 2000 sources.

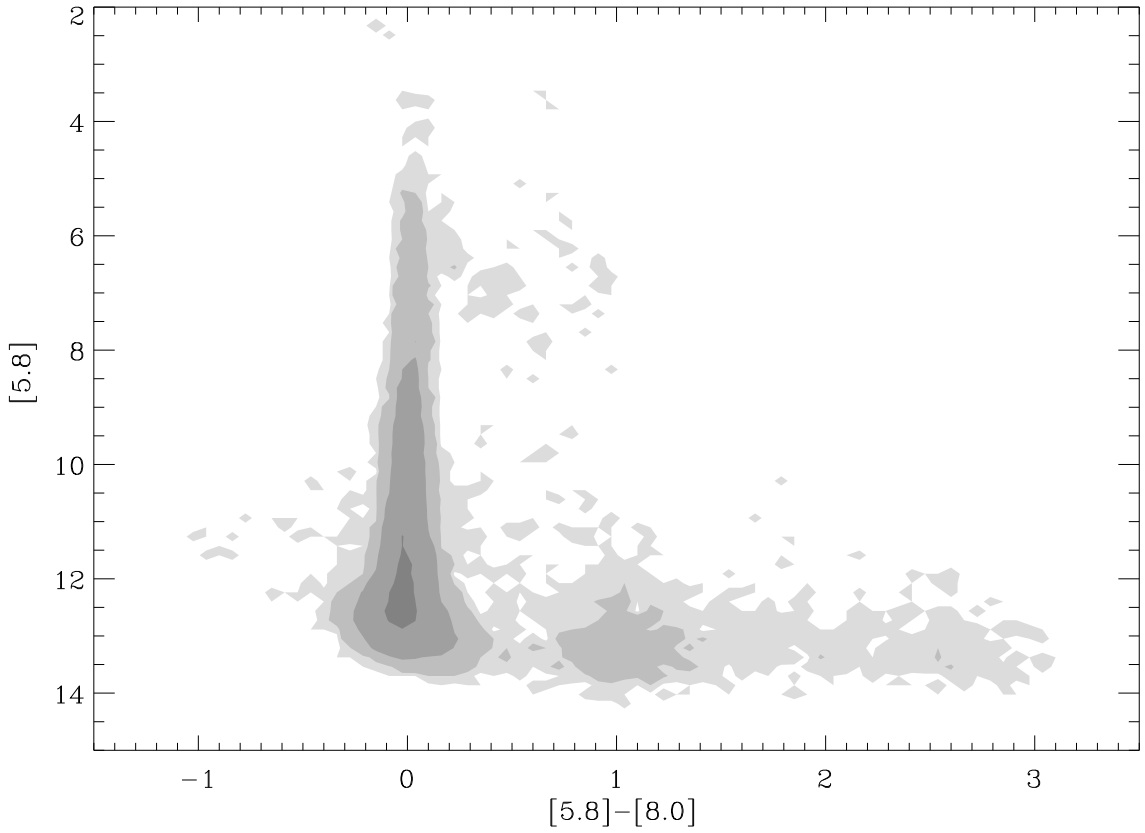

Fig. 7.— IRAC CMD for 2nd delivery catalog: [5.8] vs. [5.8]-[8.0]. Contour levels are 1, 5, 50, 500, 2000 sources.